

# Three-Dimensional Free Vibration Analysis of Thermally Loaded FGM Sandwich Plates

Vyacheslav N. Burlayenko <sup>1,†,\*</sup> , Tomasz Sadowski <sup>2</sup> and Svetlana Dimitrova <sup>3</sup>

<sup>1</sup> Department of Applied Mathematics, National Technical University 'Kharkiv Polytechnic Institute', 2 Kyrpychova Str., 61002 Kharkiv, Ukraine; burlayenko@yahoo.com

<sup>2</sup> Department of Solid Mechanics, Lublin University of Technology, 40 Nadbystrzycka Str., 20-166 Lublin, Poland; t.sadowski@pollub.pl

<sup>3</sup> Department of Higher Mathematics, National Technical University 'Kharkiv Polytechnic Institute', 2 Kyrpychova Str., 61002 Kharkiv, Ukraine; s.dimitrovaburlayenko@gmail.com

\* Correspondence: burlayenko@yahoo.com

† Current address: Department of Solid Mechanics, Lublin University of Technology, 40 Nadbystrzycka Str., 20-168 Lublin, Poland; v.burlayenko@pollub.pl

Version July 24, 2019 submitted to Materials

**Abstract:** Using the finite element code ABAQUS and the user-defined material utilities UMAT and UMATHT, a solid brick graded finite element is developed for three-dimensional (3D) modeling of free vibrations of thermally loaded functionally graded material (FGM) sandwich plates. The mechanical and thermal material properties of the FGM sandwich plates are assumed to vary gradually in the thickness direction, according to a power-law function distribution. Benchmark problems are firstly considered to assess the performance and accuracy of the proposed 3D graded finite element. Comparisons with the reference solutions revealed high efficiency and good capabilities of the developed element for the 3D simulations of thermomechanical and vibration responses of FGM sandwich plates. Some parametric studies are carried out for the frequency analysis by varying the volume fraction profile and the temperature distribution across the plate thickness.

**Keywords:** functionally graded material; sandwich plates; free vibrations; 3D graded finite element; 3D thermoelastic finite element analysis

## 1. Introduction

Sandwich panels are usually used instead of traditional structural elements made of metals and alloys, when increased strength and stiffness with little resultant weight are required for engineering applications [1–3]. Although sandwich panels provide outstanding structural features, this structural design has also drawbacks. A typical sandwich panel configuration has a high mismatch of material and geometrical properties between the face sheet and the core, [4]. Due to this, a variation of the interfacial stresses induced by thermal or/and mechanical loads is significant at the face sheet-to-core interface [5–7]. Therefore, the performance and reliability of such tri-layer composites are eventually defined by the quality of the bonded interface [8,9]. When debonding arises between the skin and core material layers, sandwich panels significantly lose their load bearing capacity [10,11]. The modal dynamic characteristics of such panels damaged by debonding are changed [12–15] and their overall dynamic responses are modified [16–19] as well. Moreover, the debonding may cause eventual failure of the sandwich panels [20–22] under dynamic loads.

In regards to reducing or avoiding the debonding issue, functionally graded materials (FGMs), with mechanical and thermal properties that are smoothly distributed over the volume, have potential for use as basic layers in sandwich panels. Usually, such sandwich configuration is achieved by

gradually changing the volume fraction of the FGM constituents across the sandwich plate thickness from the bottom face sheet to the top face sheet [23]. This removes the interface stress concentration and allows controlling deformation, dynamic responses and etc, by customizing the gradation profile [24–26]. Another characteristic of FGM sandwich panels, with metal and ceramic material, is that they can be used at elevated service temperatures [27,28]. This fact, however, gives rise to a new demand for providing safe operation of FGM sandwich panels in thermal environments. Therefore, an accurate description of the thermomechanical behavior of FGM sandwich plates becomes mandatory, mainly, to prevent their thermal failure, as considered for FGM coatings in [29–33], amongst the most recent studies. At the same time, the analysis of free vibrations of FGM sandwich panels subjected to temperature, in the design stage, is important for estimating their overall performance.

To date, a considerable amount of research on the behavior of FGM plates and panels under temperature loading is found in the literature. Various analytical (or semi-analytical) and numerical methods have been developed for this, as recently reviewed by [34] reporting that there is intense research activity with respect to modeling thermally loaded FGM composites because reliable and practical analysis procedures, in terms of accuracy and computational efforts, are in high demand. In this regard, the development of two-dimensional (2D) models is motivated by computational efficiency, e.g., [35–39]. On the other hand, such models partially lose the accuracy of predictions due to simplifications caused by prescribing the behavior of shear deformations across the panel thickness. So-called quasi-three-dimensional theories, which adopt assumptions for both shear and normal deformations in the thickness direction, have recently been proposed as an improvement to 2D theories for more reliable analyses of FGM sandwich panels, for example, in [40–42]. Nevertheless, only three-dimensional (3D) models, which are not spoiled by any additional prescriptions inherent to 2D or quasi-3D theories, are able to address unique aspects stemming from the complex dynamic response of FGM sandwich panels, [43]. However, there are two main obstacles to the use of 3D models for predictions of FGM plates. First, analytical exact 3D solutions for FGM sandwich plates are only available for simple cases of boundary conditions and geometries [44–48]. Secondly, although the finite element method (FEM), which is one of the leading computational tools, can solve problems associated with the complex geometry and different boundary conditions, the efficiency of conventional 3D finite element models is not suitable for real-scale FGM sandwich structures. The main reason for this is the layered approach for modeling material gradient with conventional finite elements because the conventional finite element has constant elastic properties over its domain. To overcome this obstacle inherent in models with conventional finite elements, the graded finite element, which assigns the material gradation profile at the element level, must be used instead. There are two techniques to elaborate a graded finite element. A nodal approximation of element material properties with interpolation functions identical to those utilized for the displacement field is used in the first technique, for example, as done in [49,50]. The second technique is based on sampling the material properties directly at the integration points of the element, [51].

Not to mention fully coupled thermomechanical problems of FGM sandwich plates involving nonlinear material behaviors, the modal dynamics of FGM sandwich plates in thermal environments is strongly dependent on the distribution of thermal stresses across the plate thickness [52–55]. On the other hand, the thermomechanical behavior of such plates is defined by the material gradation profiles. Hence, a prerequisite for high-fidelity modeling is a precise thermoelasticity analysis of such plates with accurately prescribed FGM properties. It is well-recognized that the FEM is a powerful means for solving multiphysical thermomechanical problems. Moreover, the method has been implemented in a series of commercially available codes, for instance, ABAQUS [56] which is popular among researchers and engineers. However, the package does not provide finite elements with a spatial variation of material properties. To accomplish this, programming of externally prescribed subroutines within the package environment is required. Some existing works suggest the use of the ABAQUS UEL subroutine which implements a material gradation in the FGM plates via a user-developed finite element, for example, [57]. Although this approach gives high flexibility in modeling, it requires the

79 knowledge of an experienced user and extensive benchmarks for the performance of the element  
 80 before simulations. Another approach for the implementation of varying material properties has  
 81 been reported for ABAQUS 2D plane strain elements in [30,58,59], where the strain-stress state of  
 82 FGM pavement and the thermomechanical behavior of the FGM plate have both been analyzed. The  
 83 necessary material properties of studied functionally graded materials have been distributed at the  
 84 Gauss points by coding appropriate material user-defined subroutines such as UMAT and UMATHT.  
 85 In addition, this modeling technique has been extended to 2D plate/shell and 3D models of FGM plates  
 86 in [60,61], respectively, however, only the static bending analysis has been simulated there. Recently,  
 87 three-dimensional finite element models of FGM sandwich plates for dynamic modal analysis have  
 88 been developed in [62,63].

89 The aim of this study is to propose an efficient approach for implementing a 3-D graded finite  
 90 element into ABAQUS code to perform a computationally accurate free vibration analysis of thermally  
 91 loaded FGM sandwich plates. A novel graded finite element has been developed based on the 3D brick  
 92 graded finite element proposed for the free vibration analysis of 3D FGM sandwich plates in [62,63]. In  
 93 our study, we extend the functionality of the element to use it for modeling FGM sandwich plates under  
 94 thermal loading. First, we consider a thermomechanical analysis to compute through-the-thickness  
 95 distributions of displacements and stresses in the sandwich plates. Then, with a known thermally  
 96 induced stress state, the free vibration analysis is carried out. The 3D brick graded element has been  
 97 developed by coding a combination of the subroutines such as UMAT, UMATHT, and USDFLD similar  
 98 to the 2D thermomechanical finite element analysis presented in [59]. The performance of the proposed  
 99 3D graded element has been demonstrated by the 3D modeling of heat transfer and free vibrations  
 100 of FGM sandwich plates subjected to thermal loading. The accuracy of the graded element has been  
 101 validated by comparison with results available in the literature for FGM sandwich plates. Parametric  
 102 studies have also been carried out to determine the effect of varying volume fraction profiles and  
 103 the temperature on natural frequencies and associated mode shapes. We believe that the results of  
 104 this research can be used as a benchmarks for 2D solutions and results obtained by other numerical  
 105 methods.

## 106 2. Problem Formulation

107 For the sake of completeness, the thermomechanical problem for a continuum made of a  
 108 functionally graded material is briefly summarized in this section. Throughout the section we adopt  
 109 the usual notations used in most books on Continuum Mechanics, which can be referred to for more  
 110 details.

### 111 2.1. Thermomechanical Problem

112 Let us consider the FGM sandwich plate as a 3D deformable medium occupying the domain  
 113  $\Omega \in [0, a] \times [0, b] \times [-\frac{h}{2}, +\frac{h}{2}]$  bonded by the surface,  $\partial\Omega \subset \Omega$ , at an instant of time,  $t \in [0, t_{end}]$ . The  
 114 plate is defined at a given temperature  $T_0$  in the unstressed reference configuration with respect to  
 115 a rectangular Cartesian co-ordinate system,  $x_i = (x, y, z)$ , with the  $z$ -axis aligned along the plate  
 116 thickness and with the plane,  $z = 0$ , coinciding with the mid-plane of the sandwich plate. In addition,  
 117 the planes  $z = \pm h/2$  refer to the bottom  $\partial\Omega^-$  and the top  $\partial\Omega^+$  plate surfaces, respectively, where  
 118  $\partial\Omega \setminus (\partial\Omega^- \cup \partial\Omega^+) = [-\frac{h}{2}, +\frac{h}{2}]$ , as shown in Figure 1a.

119 In the Lagrangian description, the equations of mechanical motion and thermal equilibrium at  
 120 each spatial point,  $\mathbf{x}$ , of the domain,  $\Omega$ , at a time instant,  $t$ , in the absent of body forces and internal  
 121 heat sources can be presented as [64]:

$$\begin{aligned} \nabla \cdot \boldsymbol{\sigma} &= \rho(\mathbf{x})\ddot{\mathbf{u}}, \\ -\nabla \cdot \mathbf{q} &= \rho(\mathbf{x})c(\mathbf{x})\dot{\theta} + \beta(\mathbf{x})T_0 \text{Tr}(\dot{\boldsymbol{\epsilon}}), \end{aligned} \quad (1)$$

122 where,  $\boldsymbol{\sigma}$  and  $\mathbf{q}$  are the Cauchy stress tensor and the heat flux vector, respectively;  $\mathbf{u}$  is a displacement  
 123 field and  $\theta$  stands for a temperature field associated with a change of the instantaneous temperature

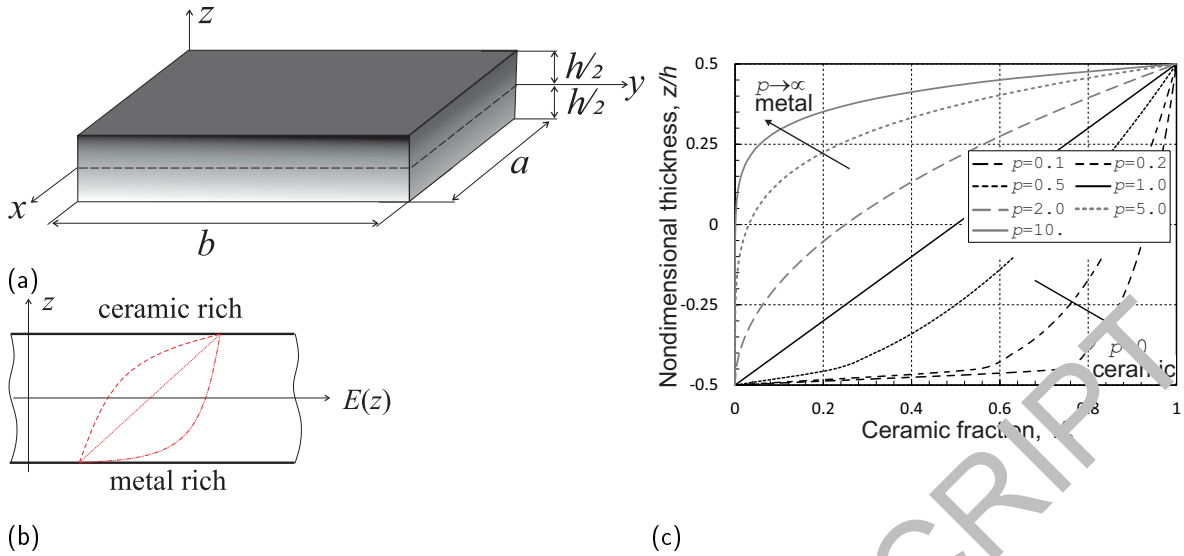


**Figure 1.** Sketches of: (a) functionally gradient material (FGM) sandwich panel; (b) through-the-thickness gradations of material properties; and (c) variations of ceramic volume fraction variations for various power-law indexes  $p$ .

124  $T(\mathbf{x}, t)$  above the reference temperature  $T_0$  at time  $t \in [0, t_{enu}]$ ; and  $\rho(\mathbf{x})$ ,  $c(\mathbf{x})$ , and  $\beta(\mathbf{x})$  denote the  
 125 mass density, the specific heat, and the stress-temperature modulus, respectively, which are functions  
 126 of a spatial position  $\mathbf{x}$ .

127 Assuming small displacements and deformations, the infinitesimal strain tensor as a sum of  
 128 elastic mechanical "el" and thermal "th" parts is expressed by

$$\begin{aligned} \boldsymbol{\varepsilon} &= \boldsymbol{\varepsilon}^{el} + \boldsymbol{\varepsilon}^{th} = \frac{1}{2} (\nabla \mathbf{u} + (\nabla \mathbf{u})^T), \\ \boldsymbol{\varepsilon}^{th} &= \alpha(\mathbf{x}) \theta \mathbf{I}, \end{aligned} \quad (2)$$

129 where  $\alpha(\mathbf{x})$  is the coefficient of thermal expansion and  $\mathbf{I}$  is the identity tensor.

130 Consider the FGM is a linear isotropic material that complies with the classical law of thermal  
 131 conductivity. Then, the thermoelastic constitutive equations of the FGM sandwich plate have a form:

$$\begin{aligned} \boldsymbol{\sigma} &= \lambda(\mathbf{x}) \text{Tr}(\boldsymbol{\varepsilon}) \mathbf{I} + 2\mu(\mathbf{x}) \boldsymbol{\varepsilon} - \beta(\mathbf{x}) \mathbf{I} \theta = \mathbf{D}(\mathbf{x}) : \boldsymbol{\varepsilon} - \beta(\mathbf{x}) \mathbf{I} \theta, \\ \mathbf{q} &= -\kappa(\mathbf{x}) \nabla \theta, \end{aligned} \quad (3)$$

132 where, the Lamé constants  $\lambda(\mathbf{x})$  and  $\mu(\mathbf{x})$  of the elasticity tensor  $\mathbf{D}(\mathbf{x})$ , the modulus  $\beta(\mathbf{x}) = \alpha(3\lambda + 2\mu)$   
 133 and the conductivity  $\kappa(\mathbf{x})$  are pointwise functions of location.

134 Two types of the boundary conditions must be specified on the plate surface  $\partial\Omega$  at any instant  
 135 in time. The mechanical boundary conditions are prescribed by displacements  $\bar{\mathbf{u}}$  on the boundary  
 136  $\partial\Omega_u$  and traction  $\bar{\mathbf{t}}$  on the boundary  $\partial\Omega_t$ , where  $\partial\Omega_t \cup \partial\Omega_u = \partial\Omega$ . In a similar manner, the thermal  
 137 boundary conditions are defined by a prescribed temperature  $\bar{T}$  and heat flux  $\bar{q}_1$  and/or an exposure  
 138 to an ambient temperature through convection so that  $\bar{q}_2 = \hat{h}(\mathbf{x})(T - T_\infty)$  on the plate surfaces  $\partial\Omega_\theta$   
 139 and  $\partial\Omega_q = \partial\Omega_{q_1} \cup \partial\Omega_{q_2}$ , respectively. Here,  $\hat{h}(\mathbf{x})$  is the heat film transfer coefficient and  $T_\infty$  is the  
 140 temperature of the surrounding medium [64].

141 Using the principle of virtual work and collecting (1) to (3) with appropriate boundary conditions,  
 142 the system of mechanical and energy equations can be rewritten in the weak form as follows:

$$\begin{aligned} \int_{\Omega} \{ \boldsymbol{\sigma} : \nabla \delta \mathbf{u} + \rho(\mathbf{x}) \ddot{\mathbf{u}} \cdot \delta \mathbf{u} \} dV - \int_{\partial\Omega_t} \bar{\mathbf{t}} \cdot \delta \mathbf{u} dA &= 0, \\ \int_{\Omega} \{ [\rho(\mathbf{x}) c(\mathbf{x}) \dot{\theta} + T_0 \beta(\mathbf{x}) \text{Tr}(\boldsymbol{\varepsilon})] \delta \theta - \mathbf{q} \cdot \nabla \delta \theta \} dV + \int_{\partial\Omega_q} \bar{\mathbf{q}} \delta \theta dA &= 0, \end{aligned} \quad (4)$$

143 for all kinematically admissible virtual displacement  $\delta \mathbf{u}$  and temperature  $\delta \theta$  fields.

## 144 2.2. Properties of FGM

145 We assume that the sandwich plate be made of a two-phase metal-ceramic functionally graded  
 146 material and, also, without loss of generality, a smooth variation of material thermomechanical  
 147 properties across the plate thickness only, i.e., in the  $z$ -direction, see Figure 1b. Herewith, it is deemed  
 148 that the face sheets (or skins) are homogeneous, i.e. pure metal on one side and pure ceramic on the  
 149 other one, with a small or negligible small thickness as compared with the thick metal-ceramic FGM  
 150 core. In addition, we suggest that the gradation profile of the ceramic volume fraction from the bottom  
 151 to top sandwich plate skins is known and is determined by a power-law function in the form:

$$V_c = V_c^- + (V_c^+ - V_c^-) \left( \frac{1}{2} + \frac{z}{h} \right)^p, \quad (5)$$

152 where,  $V_c^-$  and  $V_c^+$  are the volume fraction of ceramic on the bottom and top surfaces, respectively.  
 153 The case of  $V_c^- = 0$  and  $V_c^+ = 1$  refers to the gradation profile from pure metal on  $z = -h/2$  to pure  
 154 ceramic on  $z = +h/2$ . It follows from (5) that the FGM plate is ceramic-rich when the parameter  
 155  $p < 1$ , and metal-rich when the parameter  $p > 1$ . Figure 1c shows the volume fraction variation of the  
 156 ceramic phase along the plate thickness depending on the values of the power-law index  $p$ .

157 The effective mass density, and thermal and mechanical properties at a point of the FGM are  
 158 specified based on the "rule of mixture" as follows:

$$P(z) = P_m + (P_c - P_m)V_c \quad (6)$$

159 where,  $P(z)$  represents either the mass density or any of the thermomechanical parameters; and the  
 160 subscripts "m" and "c" are the metallic and ceramic phases whose volume fractions are such that  
 161  $V_m + V_c = 1$ . In turn, each of the parameters may depend on the temperature in the form:

$$P(T) = P_0 \left( P_{-1} \frac{1}{T} + 1 + P_1 T + P_2 T^2 + P_3 T^3 \right), \quad (7)$$

162 where,  $P_0$  stands for material parameters at the reference temperature  $T_0$  and  $P_{-1}$ ,  $P_1$ ,  $P_2$ , and  $P_3$  are  
 163 constants specifying the temperature dependence of the material at the instantaneous temperature  $T$ .

164 Finally, since the gradient in properties occurs only along the plate thickness direction, then the  
 165 material tensor in (3) in the Voigt notation is as follows:

$$\mathbf{D}(z) = \begin{bmatrix} 2\mu(z) + \lambda(z) & \lambda(z) & \lambda(z) & & & \\ \lambda(z) & 2\mu(z) + \lambda(z) & \lambda(z) & & & \\ \lambda(z) & \lambda(z) & 2\mu(z) + \lambda(z) & & & \\ & & & \mu(z) & & \\ & & & & \mu(z) & \\ & & & & & \mu(z) \end{bmatrix} \quad (8)$$

## 166 3. Method of Solution

167 A displacement-based FEM framework is used for solving the problem formulated in Section 2.

### 168 3.1. Finite Element Discretization

169 In the context of FEM, the actual continuous model of the sandwich plate is idealized by an  
 170 assemblage of arbitrary non-overlapping finite elements,  $\Omega = \bigcup_{e=1}^N \Omega^e$ , interconnected at nodal points.  
 171 For each base element, the displacement vector,  $\mathbf{u}^{(e)}$ , and a scalar function of temperature,  $\theta^{(e)}$ , are  
 172 approximated by suitable interpolation functions such that

$$\begin{aligned} \mathbf{u}^{(e)}(\mathbf{x}, t) &= \mathbf{N}(\mathbf{x})\mathbf{U}^{(e)}(t), \\ \theta^{(e)}(\mathbf{x}, t) &= \tilde{\mathbf{N}}(\mathbf{x})\Theta^{(e)}(t) \end{aligned} \quad (9)$$

173 Here, the summation over all nodal points of the base element is intended, also,  $\mathbf{N} = [N_I(\mathbf{x})]$  and  
 174  $\tilde{\mathbf{N}} = [N_P(\mathbf{x})]$  are matrices of the shape functions  $N_I$  and  $N_P$  for the displacements and the temperature,  
 175 respectively, associated with certain nodes  $I$  and  $P$ . The vectors  $\mathbf{U}^{(e)}$  and  $\Theta^{(e)}$  are the nodal unknown  
 176 displacements and temperature at those nodes.

177 The coupling between the mechanical and thermal problems is assumed to be due to the  
 178 temperature only, i.e., there is no feedback on the energy expression through the displacement field.  
 179 This assumption is reasonable if a thermomechanical model is used that does not involve internal  
 180 variables, such as plastic strains for computing the energy dissipation rate [56]. Substituting the  
 181 displacement and temperature approximations (9) into the variational equalities (4) and accounting  
 182 for the material laws in (3), we arrive at the system of semidiscrete equations of a one-way  
 183 thermomechanical problem at the element level as follows:

$$\begin{bmatrix} \mathbf{M}^{(e)} & \mathbf{0} \\ \mathbf{0} & \mathbf{0} \end{bmatrix} \begin{Bmatrix} \ddot{\mathbf{U}}^{(e)} \\ \ddot{\Theta}^{(e)} \end{Bmatrix} + \begin{bmatrix} \mathbf{0} & \mathbf{0} \\ \mathbf{0} & \mathbf{C}^{(e)} \end{bmatrix} \begin{Bmatrix} \dot{\mathbf{U}}^{(e)} \\ \dot{\Theta}^{(e)} \end{Bmatrix} + \begin{bmatrix} \mathbf{K}_u^{(e)} & \mathbf{K}_{u\theta}^{(e)} \\ \mathbf{0} & \mathbf{K}_\theta^{(e)} \end{bmatrix} \begin{Bmatrix} \mathbf{U}^{(e)} \\ \Theta^{(e)} \end{Bmatrix} = \begin{Bmatrix} \mathbf{F}_u^{(e)} \\ \mathbf{F}_\theta^{(e)} \end{Bmatrix} \quad (10)$$

184 Forms of the element matrices involved in (10) are found, for example, in [39].

185 The assembly operation  $(\bullet) = \sum_{e=1}^N (\bullet)$  over all the finite elements leads to the global system of  
 186 semidiscrete equations for the thermoelastic problem in the form:

$$\begin{bmatrix} \mathbf{M} & \mathbf{0} \\ \mathbf{0} & \mathbf{0} \end{bmatrix} \begin{Bmatrix} \ddot{\mathbf{U}} \\ \ddot{\Theta} \end{Bmatrix} + \begin{bmatrix} \mathbf{0} & \mathbf{0} \\ \mathbf{0} & \mathbf{C} \end{bmatrix} \begin{Bmatrix} \dot{\mathbf{U}} \\ \dot{\Theta} \end{Bmatrix} + \begin{bmatrix} \mathbf{K}_u & \mathbf{K}_{u\theta} \\ \mathbf{0} & \mathbf{K}_\theta \end{bmatrix} \begin{Bmatrix} \mathbf{U} \\ \Theta \end{Bmatrix} = \begin{Bmatrix} \mathbf{F}_u \\ \mathbf{F}_\theta \end{Bmatrix} \quad (11)$$

187 where,  $\mathbf{M}$ ,  $\mathbf{K}_u$ ,  $\mathbf{K}_\theta$  and  $\mathbf{C}$  are the usual global mass, stiffness, conductivity, and capacity matrices,  
 188 respectively;  $\mathbf{K}_{u\theta}$  is the coupling thermoelasticity matrix;  $\mathbf{U}$  and  $\Theta$  are the global vectors of nodal  
 189 displacements and nodal temperature, the derivatives of them correspond to the time derivatives of these  
 190 vectors; and  $\mathbf{F}_u$  and  $\mathbf{F}_\theta$  are global vectors of the mechanical and thermal forces.

191 In the case of an uncoupled formulation the temperature is given as an external load and it is  
 192 not a primary variable in the mechanical analysis. More specifically, the thermal virtual work leads  
 193 to the initial stress matrix known as a geometric stiffness matrix  $\mathbf{K}_G$ , which contains the terms due  
 194 to the temperature loading on the leading diagonal. Thus, first, the temperature field is computed at  
 195 the given thermal and displacement boundary conditions. Then, a temperature profile, known for  
 196 solving the mechanical problem with the same displacement boundary conditions, is used to find  
 197 the displacement and stress fields. The nonlinear finite element equations of the thermomechanical  
 198 problem are solved by an iterative method, where the nonlinear terms of linearized equations are  
 199 evaluated as a known solution from the preceding iteration. The Newton-Raphson iterative method is  
 200 used in ABAQUS [56]. Finally, the frequency analysis, which accounts for the initial deformed state  
 201 associated with the temperature-induced stresses, is carried out by extracting natural frequencies from  
 202 the eigenvalue-type equation:

$$\left( (\mathbf{K} + \mathbf{K}_G) - \omega^2 \mathbf{M} \right) \boldsymbol{\phi} = 0, \quad (12)$$

203 where  $\omega$  is an undamped circular frequency and  $\boldsymbol{\phi}$  is a vector associated with mode shape at a specific  
 204 frequency  $\omega$ .

### 205 3.2. Three-Dimensional Graded Element

206 The thermomechanical analysis and the modal frequency extraction procedure for FGM sandwich  
 207 plates are carried out with the ABAQUS/Standard code using three-dimensional models. Since  
 208 conventional 3D finite elements, which are available in the ABAQUS finite element library, are not  
 209 able to model a variation of the thermal and mechanical properties within the element volume, a 3D  
 210 graded finite element incorporating gradients of material properties is developed.

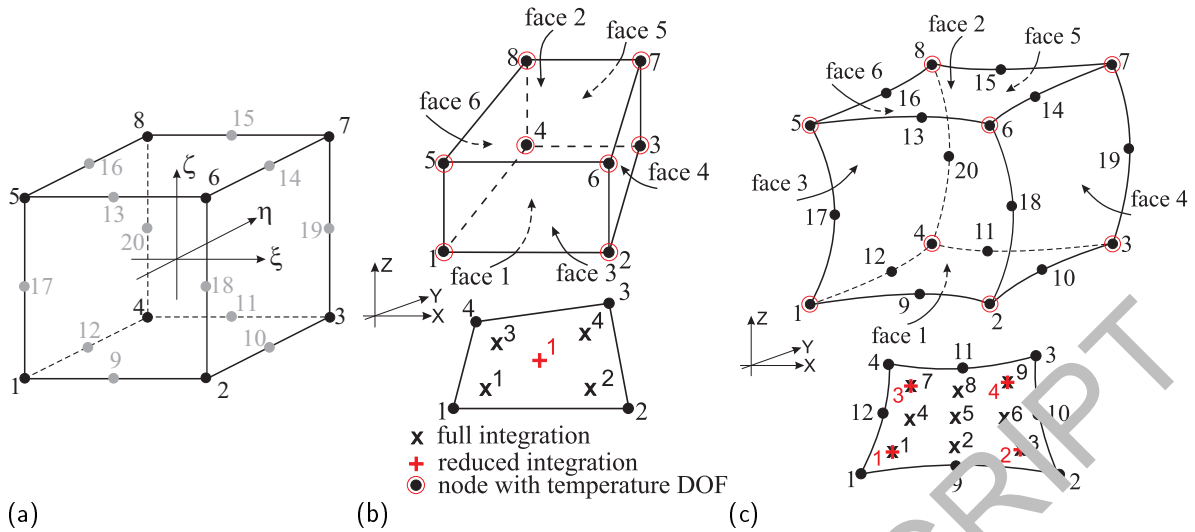


**Figure 2.** Isoparametric 3-D brick finite elements form [56]: (a) master element; (b) eight-node linear element with reduced and full integration schemes<sup>1</sup>; and (c) 20-node quadratic element with reduced and full integration schemes<sup>1</sup>.

<sup>1</sup> Numbering of integration points for output is shown in the element layer closest to the face 1, and the integration points in the other layers are numbered consecutively.

211 As mentioned in the Introduction, a 3D graded finite element has been developed for performing  
 212 the modal frequency analysis of FGM sandwich plates in [62,63]. To incorporate a variation in the elastic  
 213 properties of the heterogeneous material into the finite element, the material user-defined subroutine  
 214 UMAT that establishes the tangent element stiffness matrix was programmed, while the average mass  
 215 density value was adopted to determine the element mass matrix. In our study, the performance of  
 216 the 3D graded finite element is extended to provide thermal loading and temperature-dependent  
 217 material properties for carrying out the thermomechanical analysis of the FGM sandwich plates. Such  
 218 an analysis requires computing and storing the internal thermal energy and the heat flux which comply  
 219 with the energy balance equation (1) and Fourier's law of heat conduction (3), respectively, as well as  
 220 modifying the mechanical behavior by accounting for thermal strains (2). The implementation of a  
 221 spatial variation of the thermal and modified mechanical properties in the selected direction in the 3D  
 222 graded finite element has been done following the procedure outlined in [59] for a 2D graded finite  
 223 element. With this approach, a master 3D temperature-displacement finite element, either eight-node  
 224 linear C3D8 or twenty-node quadratic C3D20 brick isoparametric element with either reduced or  
 225 fully integration scheme, which are available in ABAQUS (Figure 2), has been supplemented by a  
 226 combination of user-defined subroutines such as UMAT, UMATHT, and USDFLD, [56]. In addition,  
 227 it should be mentioned that ABAQUS interpolates the temperature field using only the first-order  
 228 approximation regardless of the order of approximation of the displacement field, as shown in Figure 2b  
 229 and c.

230 The material subroutine UMAT was programmed to define a through-the-thickness variation  
 231 of the Lamé constants,  $\lambda(\mathbf{x})$  and  $\mu(\mathbf{x})$ , and the stress-temperature modulus,  $\beta(\mathbf{x})$ , associated with  
 232 the thermal expansion coefficient,  $\alpha(\mathbf{x})$ . The distributions across the thickness of the material  
 233 thermal properties were incorporated into the element by coding the specific heat,  $c(\mathbf{x})$ , the thermal  
 234 conductivity,  $\kappa(\mathbf{x})$ , and the film heat transfer,  $\hat{h}(\mathbf{x})$ , coefficients in the UMATHT subroutine. Finally,  
 235 the through-the-thickness variation of mass density was incorporated into the element using the  
 236 USDFLD subroutine. Moreover, if the material parameters were deemed to exhibit a temperature  
 237 dependence, appropriate relationships (7) with given coefficients for each material parameter were  
 238 also programmed as functions of the temperature in the mentioned subroutines. In doing so, the  
 239 instantaneous temperature,  $T$ , was known as it is a variable passed for information at each time

240 increment in the subroutines, and therefore, the property was able to be computed at any current  
241 temperature value.

242 By running the ABAQUS code, the element matrices, presented in (10), which involve variations  
243 of the material thermal and mechanical properties coded in accordance with a certain relation for FGM  
244 constituents, have been generated by calling the corresponding user-defined subroutines. Thus, the  
245 material properties that account for the given material gradation profiles have been assigned directly at  
246 the Gauss integration points of the element (see Figure 2b and c). In such a way, any arbitrary material  
247 gradient, for example, a power-law distribution of the ceramic phase in the thickness direction of the  
248 plate can be prescribed. More details of the implementation of graded elements into the ABAQUS  
249 code are found in [30,59] and the ABAQUS manual [56]. In addition, it is important to note that the  
250 mass density, averaged over the FGM sandwich plate volume [62,63], was used in the free vibration  
251 analysis instead of its spatial representation in the case of thermomechanical analysis.

#### 252 4. Comparison Study

253 The performance of the 3D graded element described above for solving thermomechanical and  
254 free vibration problems has been verified by comparing calculated numerical solutions with results  
255 available in the literature.

##### 256 4.1. Cube Problem

257 As a first validation problem, a unit FGM cube ( $L = 1$ ), that has been subjected to prescribed  
258 temperatures on two opposite sides and insulated in all the other sides is considered, Figure 3a. This  
259 problem has been solved analytically and numerically using the boundary element method in [65]. The  
260 top surface of the cube  $z = 1$  is maintained at the temperature  $T_L = 100^\circ\text{C}$ , while the temperature of  
261 the bottom surface at  $z = 0$  is  $0^\circ\text{C}$ . The reference temperature is also assumed to be  $0^\circ\text{C}$ . The variations  
262 of thermal conductivity and specific heat along the  $z$ -axis are defined by the expressions:

$$\kappa(z) = \kappa_0 e^{2\zeta z} = \kappa e^{2z} \quad \text{and} \quad c(z) = c_0 e^{2\zeta z} = e^{2z}$$

263 The analytical solution for the temperature in the transient thermal analysis is known [65] as

$$\theta(z, t) = T_L \frac{1 - e^{-2\zeta z}}{1 - e^{-2\zeta L}} + \sum_{n=1}^{\infty} B_n \sin\left(\frac{\pi n z}{L}\right) e^{-\zeta z} e^{-\left(\frac{\pi^2 n^2}{L^2} + \zeta^2\right) e t},$$

264 where, the coefficients,  $B_n$ , are given in the form:

$$B_n = -T_L \frac{2e^{\zeta L}}{\zeta^2 L^2 + \pi^2 n^2} \left[ \zeta L \sin(\pi n) \frac{1 + e^{-2\zeta L}}{1 - e^{-2\zeta L}} - \pi n \cos(\pi n) \right] \quad \text{and} \quad \epsilon = \kappa_0 / c_0$$

265 In the finite element simulations, the cube is discretized with  $4 \times 4 \times 4$  twenty-node quadratic  
266 brick graded elements, as illustrated by Figure 3b. A transient heat transfer analysis is performed with  
267 ABAQUS, calling the material subroutines UMATHHT and USDFLD. The temperature profile along  
268 the  $z$ -axis is plotted at different times for the given exponential material variations and compared  
269 with the analytical solutions, as shown in Figure 3c. It is evident from the plot that the numerical and  
270 analytical results are in excellent agreement.

##### 271 4.2. Analysis of FGM plates

272 As a second example, an aluminum-zirconia functionally graded square plate with sides  $a = b =$   
273  $0.2$  m and thickness  $h = 0.01$  m, as studied in [35] is considered. The plate is assumed to be simply  
274 supported on all the edges and is exposed to a temperature field such that the ceramic-rich top surface  
275 is held at  $300^\circ\text{C}$  and the metal-rich bottom surface is held at  $20^\circ\text{C}$ . A stress-free state is assumed to  
276 be at  $0^\circ\text{C}$ . The material thermomechanical parameters of the FGM plate are listed in Table 1. For the  
277 purpose of comparison, the values of the volume fraction exponent,  $p$ , in (5) have been accepted as 0.0

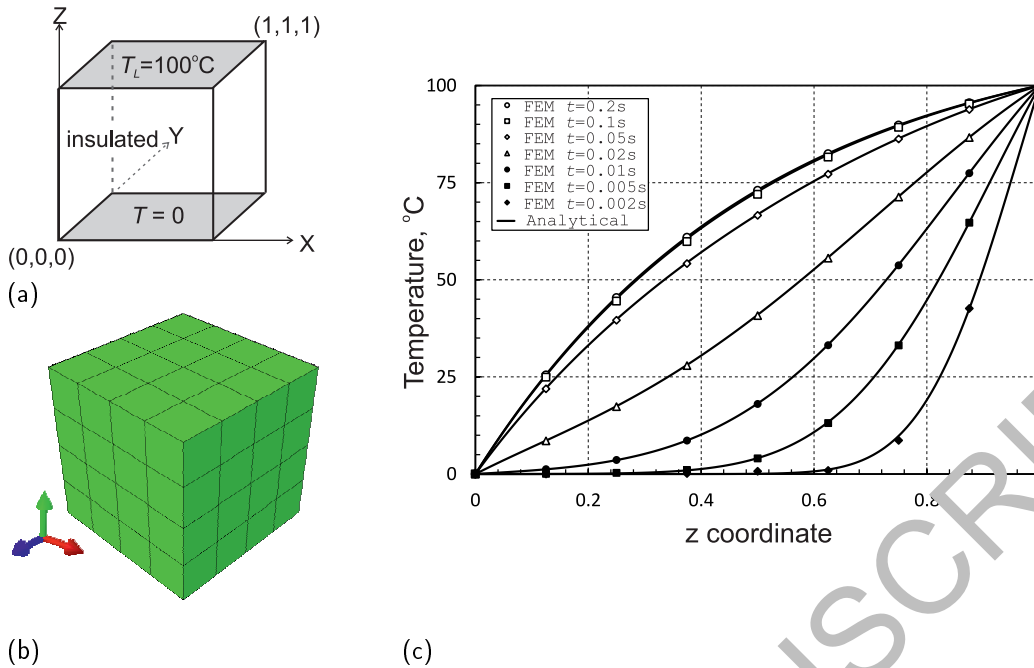


**Figure 3.** The FGM unit cube problem: (a) geometry and thermal boundary conditions, (b) finite element mesh, and (c) transient temperature profiles.

278 (pure ceramic), 0.2, 0.5, 1.0, 2.0 and  $\infty$  (pure metal). Figure 4a shows the variation of the temperature  
 279 through-the-thickness profiles of the FGM plate depending on the exponent values. By comparing the  
 280 temperature profiles shown in Figure 4a with those illustrated in [35] (p. 680), one can conclude that  
 281 the plots are nearly identical.

**Table 1.** Material properties of FGM constituents.

Constants	Aluminum	Zirconia( $ZrO_2$ )	Steel(SUS304)	Silicon( $Si_3Ni_4$ )
E, GPa	70.0	151.0	201.04	348.43
$\nu$	0.3	0.3	0.3262	0.24
$\rho$ , kg/m <sup>3</sup>	2707	3000	8166	2370
$\kappa$ , W/m	204.0	2.09	12.04	9.19
c, J/kgK	896.0	274.0	555.11	496.56
$\alpha \times 10^{-6}$ , /°C	23.0	10.0	12.33	5.87

282 With these calculations it was found that the calculated results converge to the reference data in  
 283 [35] with an increase of the number of graded elements in the thickness direction. The best agreement  
 284 between both the solutions was achieved using eight graded elements across the plate thickness. This  
 285 resulted in time-consuming computations in the case of cubic elements used in the mesh. In order too  
 286 speed up the computations, brick graded elements, with an aspect ratio 4:4:1, have been used instead.  
 287 The elements provided more than 10 times faster computations with the same through-the-thickness  
 288 profiles for variations of temperature and quite acceptable results for temperature-induced deflections  
 289 and stresses across the thickness, as illustrated in Figure 4b-f, respectively, as compared with those in  
 290 [44]. Therefore, such elements are used in the calculations to follow.

291 As shown in Figure 4a, it is obvious that the metal and ceramic plates have linear temperature  
 292 variations through-the-thickness profiles, while the FGM plates possess non-linear temperature profiles  
 293 with much lower temperatures in the bottom part of the plate thickness due to the insulation effect of  
 294 ceramic located over the metallic part. Nevertheless, although FGM plates have intermediate properties  
 295 between the pure ceramic and metal plates, their central deflections do not show intermediate values  
 296 between those of the homogeneous plates, as seen in Figure 4b. This is related to the fact that the

deflection depends on the product of the temperature and the thermal expansion coefficient. The latter is larger in the metal-rich region, while the temperature is higher in the ceramic-rich portion. As a result, the thermal strains are not uniform over the plate thickness and the responses of the FGM plates are not intermediate to those of the pure metal and ceramic plates. The temperature-induced through-the-thickness distributions of central longitudinal and transverse normal stresses, and a transverse shear stress at the center of plate edge and an in-plane shear stress at the plate corner, shown in Figure 4c - f, respectively, demonstrate that the longitudinal normal stresses in the FGM plates exhibit nonlinear profiles in contrast to linear ones in the pure metal and ceramic plates, whereas, the transverse normal stress and the shear stresses of all the plates have rather similar profiles and in the case of FGM plates, the stress distributions crucially depend on the power-law index  $p$ .

In order to evaluate the accuracy of the developed graded element in the free vibration analysis of thermally loaded FGM plates, the natural frequencies of a fully clamped (CCCC) square FGM plate with the thickness-side ratio  $h/a = 0.1$  have been computed and compared with the available in [46]. Steel-silicon SUS304/Si<sub>3</sub>Ni<sub>4</sub> functionally graded plates were considered. The properties of constituents of the FGM are given in Table 1, while the temperature-dependent constants of the constituents can be found in [46] (p. 737, Table 1). The FGM plates were assumed to be subjected to different temperatures equal to 300 K, 600 K and 800 K, which are uniformly distributed across the plate thickness. The natural frequencies of the FGM plates extracted from the finite element analysis have been nondimensionalized as follows:

$$\bar{\omega} = \frac{\omega a^2}{\pi^2} \sqrt{\frac{I_m}{D_m}}$$

where,  $I_m = h\rho_m$  and  $D_m = E_m h^3 / (12(1 - \nu_m^2))$  are expressed using the appropriate values of the stainless steel at the reference temperature  $T_0 = 300$  K. Table 2 shows a good agreement between the computed nondimensional frequencies ( $\omega_{FEM}$ ) and the results ( $\omega_{Ref.}$ ) reported in [46].

**Table 2.** Comparisons of nondimensional frequencies for a fully clamped (CCCC) SUS304/Si<sub>3</sub>Ni<sub>4</sub> functionally graded square plate thermally loaded by the uniform temperature rise,  $T$ .

$T$	$p$	Source	$\bar{\omega}_1$	$\bar{\omega}_2 = \bar{\omega}_3$	$\bar{\omega}_4$	$\bar{\omega}_5$	$\bar{\omega}_6$	$\bar{\omega}_7 = \bar{\omega}_8$
300 K	2	Present	4.1677	7.9565	11.1587	13.1533	13.2784	15.6883
		Li et al. [46]	4.1658	7.9389	11.1212	13.0973	13.2234	15.3627
		$\Delta, \%$	0.0449	0.221	0.337	0.427	0.416	2.119
600 K	2	Present	3.7587	7.3978	10.4864	12.4164	12.5484	15.0855
		Li et al. [46]	3.7202	7.301	10.3348	12.2256	12.3563	14.8112
		$\Delta, \%$	1.035	1.326	1.467	1.560	1.554	1.852
800 K	2	Present	3.3445	6.8162	9.7681	11.6169	11.7545	14.1711
		Li et al. [46]	3.2741	6.6509	9.5192	11.3126	11.4468	13.7907
		$\Delta, \%$	2.151	2.486	2.614	2.670	2.688	2.759

$$^1 \Delta = |\omega_{Ref.} - \omega_{FEM}| / \omega_{Ref.} \times 100\%.$$

## 5. Parametric Study

After establishing the correctness of the developed 3D graded finite element, parametric studies are performed to investigate the effects of gradation profiles in thermo-elastic properties and temperature distributions on the free vibrations of FGM sandwich plates.

First, we consider the free vibration analysis of SUS304/Si<sub>3</sub>Ni<sub>4</sub> functionally graded square sandwich plates with the skins' thickness negligible as compared with the core thickness. The geometry and material properties of the sandwich plates were identical to the analysis for the FGM plate in Section 4.2. It is assumed that across the thickness, the sandwich plates may be subjected to either a uniform temperature field,  $T_b = T_t = T$ , or a temperature profile associated with a steady-state heat

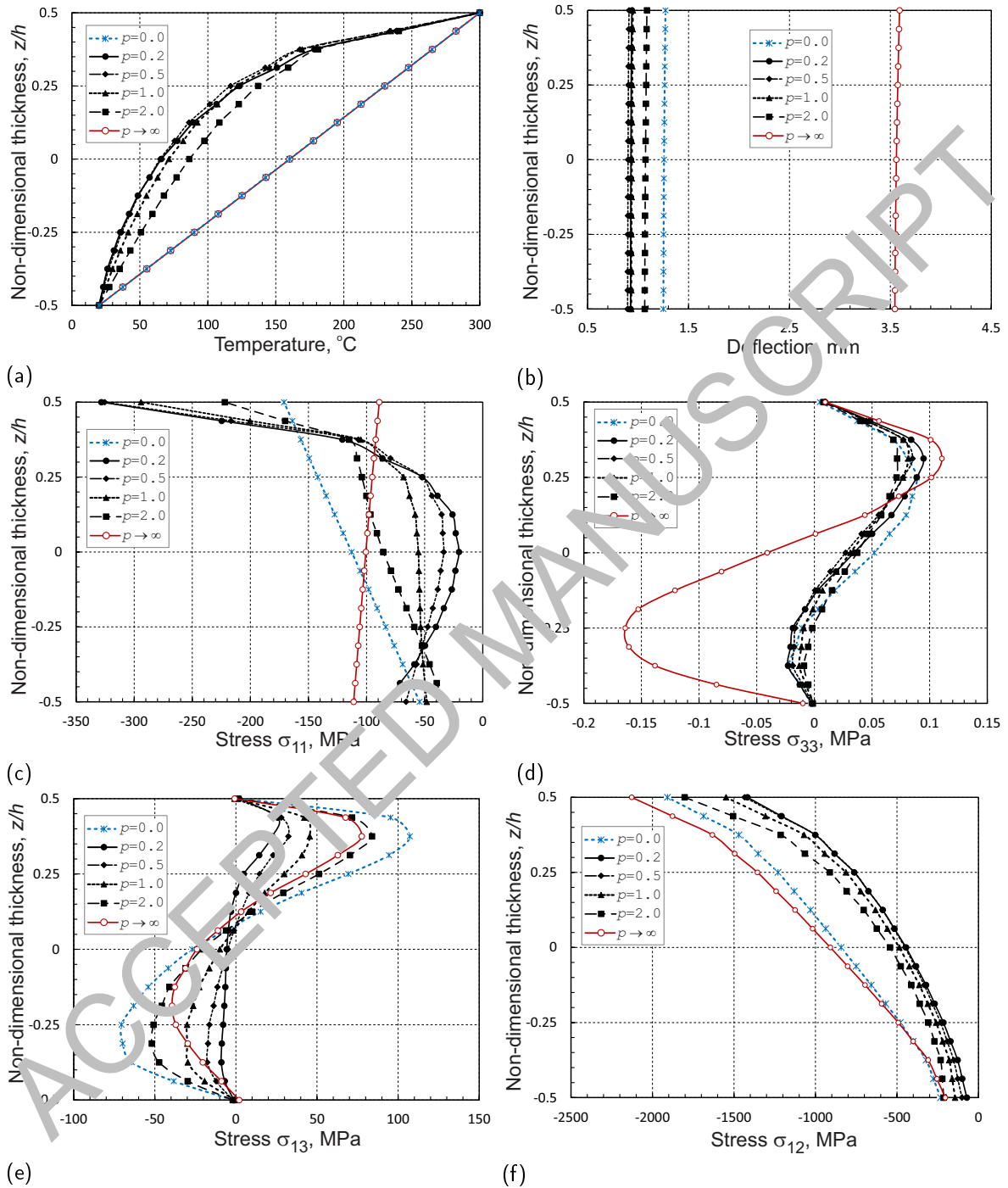


**Figure 4.** Through the thickness profiles of: (a) temperature at  $(\frac{a}{2}, \frac{b}{2}, z)$ ; (b) deflection at  $(\frac{a}{2}, \frac{b}{2}, z)$ ; (c) longitudinal normal stress  $\sigma_{11}$  at  $(\frac{a}{2}, \frac{b}{2}, z)$ ; (d) transverse normal stress  $\sigma_{33}$  at  $(\frac{a}{2}, \frac{b}{2}, z)$ ; (e) transverse shear stress  $\sigma_{13}$  at  $(0, \frac{b}{2}, z)$ ; and (f) in-plane shear stress  $\sigma_{12}$  at  $(0, 0, z)$  in the simply supported aluminum-zirconia FG square plate.

transfer due to differently prescribed temperatures on the bottom,  $T_b$ , and top,  $T_t$ , plate surfaces. Two types of boundary conditions, i.e., all edges simply supported (SSSS) and all edges clamped are used in the calculations. Five different material gradations defined by the power-law index  $p=0.2, 0.5, 1, 5$  and 10 as well as pure ceramic ( $p=0$ ) and metal ( $p \rightarrow \infty$ ) homogeneous plates are examined. In Tables 3 and 4, the first ten nondimensional natural frequencies  $\bar{\omega}$  of simply supported and clamped FGM plates under the uniform temperature of  $T=600$  K are presented, respectively. In addition, in Tables 3 and 4, the frequencies calculated with the 3D graded elements are compared with those available in [46] for the studied FGM plates.

**Table 3.** The first ten nondimensional frequencies of simply supported (SSSS) SUS304/Si<sub>3</sub>Ni<sub>4</sub> functionally graded square plates thermally loaded by the uniform temperature rise,  $T = 600$  K.

$p$	Source	$\bar{\omega}_1$	$\bar{\omega}_2 = \bar{\omega}_3$	$\bar{\omega}_4 = \bar{\omega}_5$	$\bar{\omega}_6$	$\bar{\omega}_7$	$\bar{\omega}_8$	$\bar{\omega}_9$	$\bar{\omega}_{10}$
0.0		4.1740	10.1983	15.1457	15.7639	19.2859	19.3065	21.4208	24.2877
0.2		3.3782	8.2814	12.2937	12.8114	15.6802	15.6970	17.7655	19.7542
0.5		2.8570	7.0289	10.4044	10.8797	13.3194	13.3356	14.7118	16.7821
1	Present	2.4894	6.1445	9.0147	9.5105	11.6424	11.6418	12.7449	14.6637
	Li et al. [46]	2.5511	6.1761	8.7623	9.5119	11.6301			
	$\Delta, \%$	2.419	0.512	2.881	0.0147	0.1056			
2	Present	2.2199	5.4930	7.9240	8.4946	10.3932	10.4118	11.2017	13.0762
	Li et al. [46]	2.2690	5.4984	7.7231	8.4675	10.3536			
	$\Delta, \%$	2.163	0.0979	2.601	0.320	0.332			
5	Present	2.0077	4.9736	7.0232	7.6815	9.2911	9.4105	9.9295	11.8002
	Li et al. [46]	2.0433	4.9538	6.8769	7.6257	9.2910			
	$\Delta, \%$	1.744	0.399	2.128	0.732	0.719			
10	Present	1.9138	4.7435	6.6588	7.2267	8.9576	8.9762	9.4157	11.2552
	Li et al. [46]	1.9323	4.6881	6.4908	7.2291	8.8282			
	$\Delta, \%$	0.958	1.183	2.589	1.190	1.466			
$\infty$		1.7644	4.3928	6.2440	6.8006	8.3256	8.3435	8.8315	10.4772

**Table 4.** The first ten nondimensional frequencies of fully clamped (CCCC) SUS304/Si<sub>3</sub>Ni<sub>4</sub> functionally graded square plates thermally loaded by the uniform temperature rise,  $T = 600$  K.

$p$	Source	$\bar{\omega}_1$	$\bar{\omega}_2 = \bar{\omega}_3$	$\bar{\omega}_4$	$\bar{\omega}_5$	$\bar{\omega}_6$	$\bar{\omega}_7 = \bar{\omega}_8$	$\bar{\omega}_9 = \bar{\omega}_{10}$
0.0		9.1540	13.9341	19.7056	23.3259	23.5522	28.3132	28.3297
0.2		5.7864	11.3046	16.0039	18.9544	19.1406	23.0291	23.1370
0.5		4.8856	9.5742	13.5667	16.0738	16.2347	19.5350	19.7144
1	Present	4.2411	8.3332	11.8143	13.9971	14.1410	17.0117	17.2036
	Li et al. [46]	4.2110	8.2429	11.6602	13.7916	13.9366	16.6856	
	$\Delta, \%$	0.715	1.096	1.321	1.490	1.467	1.955	
2	Present	3.7587	7.3978	10.4864	12.4164	12.5484	15.0855	15.2405
	Li et al. [46]	3.7202	7.3010	10.3348	12.2256	12.3563	14.8112	
	$\Delta, \%$	1.035	1.326	1.467	1.560	1.554	1.852	
5	Present	3.3769	6.6504	9.4212	11.1452	11.2674	13.5341	13.6255
	Li et al. [46]	3.3267	6.5424	9.2647	10.9594	11.0790	13.2936	
	$\Delta, \%$	1.508	1.650	1.689	1.695	1.701	1.809	
10	Present	3.2164	6.3386	8.9808	10.6247	10.7418	12.9026	12.9716
	Li et al. [46]	3.1398	6.1857	8.7653	10.3727	10.4866	12.5971	
	$\Delta, \%$	2.439	2.472	2.458	2.429	2.434	2.425	
$\infty$		2.9706	5.8867	8.3613	9.9088	10.0175	12.0478	12.2222

Similar to the previous study, the first ten nondimensional natural frequencies of simply supported and clamped FGM plates subjected to the temperature profiles following from the solution of the thermomechanical analysis under steady-state conditions with the prescribed temperature on the top (ceramic) surface  $T_t=600$  K and at the reference temperature on the bottom (metal) surface  $T_b = T_0=300$  K are collected in Tables 5 and 6, respectively. The contour plot of the temperature

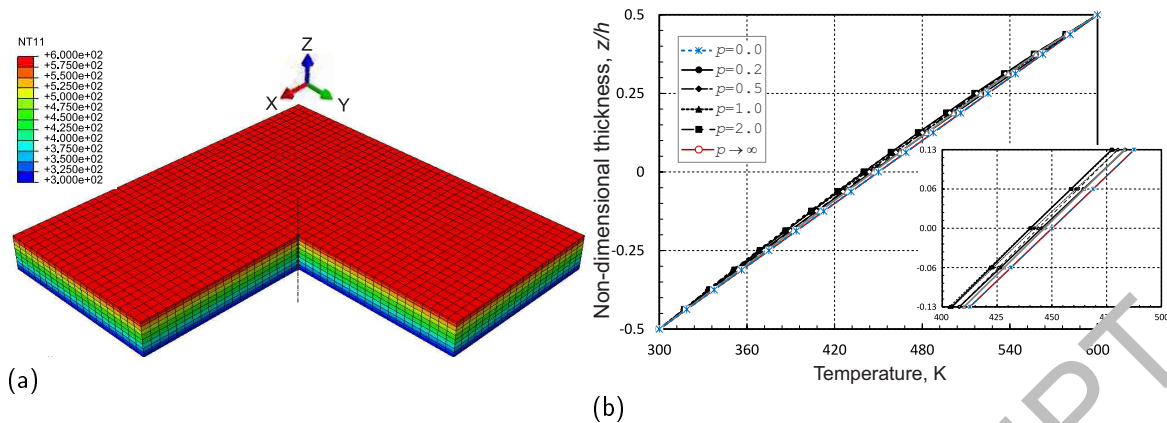


**Figure 5.** For simply supported and clamped plates: (a) temperature distribution, and (b) through-the-thickness profiles of the temperature.

341 distribution within the plate (a quarter of plate is removed from the presentation to illustrate the  
 342 temperature distribution inside the plate) and the variations of temperature across the thickness (at  
 343 the central section of the plate) depending on the power-law index  $p$ , which have been predicted by  
 344 the thermomechanical analysis for the SSSS and CCCC plates, are illustrated in Figures 5a and b. It  
 345 is evident from the latter plot that the effect of  $p$  is not significant for this material and the nonlinear  
 346 temperature profiles are very close to the linear temperature distribution.

**Table 5.** The first ten nondimensional frequencies of SSSS  $\text{Si}_3\text{Si}_2\text{O}_5/\text{Si}_3\text{Ni}_4$  functionally graded square plates thermally loaded by the nonlinear temperature rise as shown in Figure 5.

$p$	Source	$\bar{\omega}_1$	$\bar{\omega}_2 = \bar{\omega}_3$	$\bar{\omega}_4 = \bar{\omega}_5$	$\bar{\omega}_6$	$\bar{\omega}_7$	$\bar{\omega}_8$	$\bar{\omega}_9$	$\bar{\omega}_{10}$
0.0		4.3081	10.4080	15.3395	16.0514	19.6133	19.6228	21.6944	24.6815
0.2		3.5108	8.4961	12.4954	13.1047	16.0239	16.0313	17.6979	20.1604
0.5		2.9890	7.2447	10.6113	11.1745	13.6691	13.6756	15.0485	17.1928
1	Present	2.6193	6.7551	9.2251	9.7984	11.9851	11.9916	13.0976	15.0665
	Li et al. [46]	2.6576	6.7764	8.9707	9.7992	11.9555			
	$\Delta, \%$	1.443	0.334	2.836	0.008	0.247			
2	Present	2.3494	5.7002	8.1383	8.7776	10.7309	10.7370	11.5706	13.4738
	Li et al. [46]	2.3727	5.6933	7.9300	8.7468	10.6709			
	$\Delta, \%$	0.985	0.121	2.627	0.352	0.562			
5	Present	2.1123	5.1904	7.2430	7.9747	9.7453	9.7483	10.3212	12.2111
	Li et al. [46]	2.1424	5.1419	7.0806	7.8970	9.6331			
	$\Delta, \%$	0.002	0.943	2.293	0.983	1.165			
10	Present	2.0556	4.9764	6.8823	7.6380	9.3385	9.3403	9.8304	11.6898
	Li et al. [46]	2.0465	4.9106	6.7230	7.5386	9.1945			
	$\Delta, \%$	0.442	1.340	2.369	1.319	1.566			
$\infty$		1.8773	4.5577	6.4224	7.0240	8.5796	8.5865	9.0844	10.7833

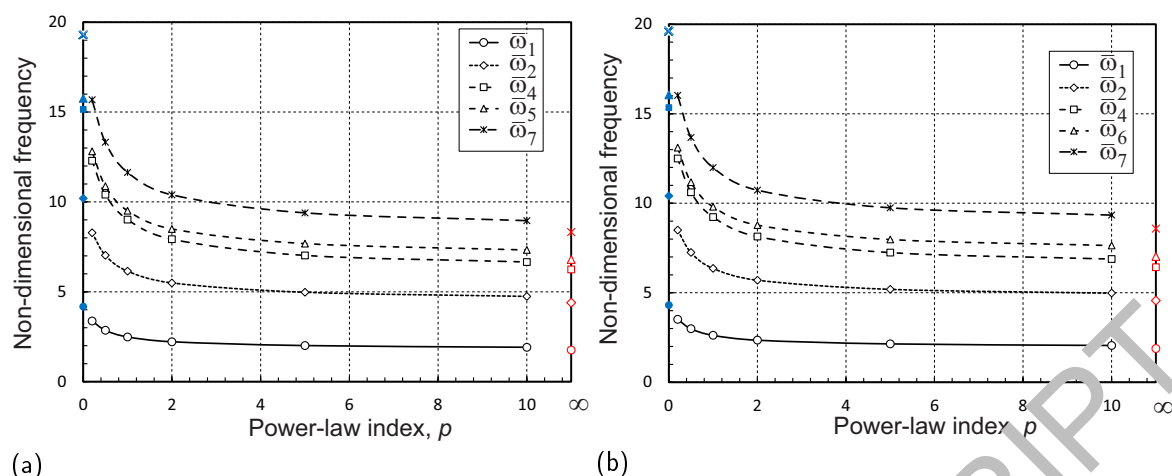


**Figure 6.** The effect of the material gradation profile on natural frequencies of: (a) SSSS plates and (b) CCCC plates.

**Table 6.** The first ten nondimensional frequencies of CCCC SUS304/Si<sub>3</sub>Ni<sub>4</sub> functionally graded square plates thermally loaded by the nonlinear temperature rise as shown in Figure 5.

$p$	Source	$\bar{\omega}_1$	$\bar{\omega}_2 = \bar{\omega}_3$	$\bar{\omega}_4$	$\bar{\omega}_5$	$\bar{\omega}_6$	$\bar{\omega}_7 = \bar{\omega}_8$	$\bar{\omega}_9 = \bar{\omega}_{10}$
0.0		7.3941	14.2773	20.1281	23.7940	24.0181	28.6535	28.8629
0.2		6.0126	11.6262	16.3992	19.3721	17.5759	23.4467	23.5288
0.5		5.1077	9.8879	13.9513	16.4991	16.6573	19.9997	20.0263
1	Present	4.4642	8.6455	12.1960	14.4167	14.5594	17.4727	17.5021
	Li et al. [46]	4.4904	8.6443	12.1579	14.3412	14.4836	17.0433	
	$\Delta, \%$	0.584	0.0137	0.330	0.540	0.523	2.520	
2	Present	3.9845	7.7113	10.8665	12.8383	12.9667	15.5080	15.5692
	Li et al. [46]	3.9965	7.6961	10.8220	12.7653	12.8934	15.1611	
	$\Delta, \%$	0.302	0.198	0.429	0.572	0.568	2.288	
5	Present	3.6006	6.9592	9.7974	11.5608	11.6791	13.8901	14.0082
	Li et al. [46]	3.5941	6.9264	9.7400	11.4873	11.6043	13.6331	
	$\Delta, \%$	0.182	0.473	0.589	0.640	0.644	1.885	
10	Present	3.4143	6.6089	9.3464	11.0290	11.1421	13.2356	13.3630
	Li et al. [46]	3.4243	6.6002	9.2799	10.9425	11.0551	12.9958	
	$\Delta, \%$	0.291	0.586	0.717	0.790	0.787	1.845	
$\infty$		3.1868	6.1832	8.7213	10.3062	10.4111	12.4894	12.4986

It is worth noting that there is very good agreement between the present results and the referenced solutions, as seen in Tables 3 to 6. This demonstrates the accuracy and effectiveness of the 3D graded finite element developed in the present work. In addition, for the sake of clear demonstration of the effect of the material gradation profile on the natural frequencies, some frequencies from Tables 5 and 6 for the simply supported and clamped FGM plates subjected to the nonlinear temperature rise are plotted as functions of the volume fraction exponent  $p$  in Figure 6a and b, respectively. It is obvious from the plots that the frequencies decrease with an increasing in the power-law index, i.e., growing the percentage of ceramic fraction in the top thickness of the FGM plates. In doing so, the higher frequencies show more intensive descending trends.

Next, sandwich plates with thickness of skins  $h_f = 0.1h$  and thickness of core  $h_c = 0.8h$ , which are referred to as 1-8-1 sandwich configurations, are considered for the free vibration analysis. Three different boundary conditions such as fully simply supported, fully clamped, and two edges simply supported and two edges clamped (SCSC) are examined. It is assumed that the sandwich plates have homogenous skins such that the top and bottom skins are pure ceramic and pure metal, respectively, and the core is SUS304/Si<sub>3</sub>Ni<sub>4</sub> functionally graded material identical to that in the previous study with the volume fraction exponent  $p=0.2, 0.5, 2$  and  $10$ . The thermomechanical constants of the

363 material constituents are listed in Table 1. The sandwich plates are assumed to be subjected to the  
 364 prescribed temperature on the top surface  $T_t$ , and the bottom surface is at the reference temperature,  
 365 i.e.,  $T_b = T_0$ . For the free vibration analyses, first, temperature gradients across the thickness of  
 366 the plates are computed using the thermomechanical analysis under steady-state conditions. Three  
 367 different temperatures  $T_t=300, 400$  and  $600$  K are applied to the ceramic surface, while the metal surface  
 368 is kept constant and equal to the reference temperature  $T_0=300$  K.

369 The nondimensional natural frequencies,  $\tilde{\omega} = \omega(a^2/h)\sqrt{\rho_m/E_m}$ , of the FGM sandwich plates for  
 370 SSSS, CCCC and SCSC boundary conditions, subjected to different temperature profiles following  
 371 from the solution of the thermomechanical analysis and for different material gradients defined by the  
 372 power-law index are tabulated in Tables 7 - 9, respectively. In Tables 7 - 9, for the sake of controlling  
 373 the accuracy of simulations, the first two frequencies have been compared with those presented in [39].

**Table 7.** The first ten nondimensional frequencies of SSSS SUS304/Si<sub>3</sub>Ni<sub>4</sub> functionally graded square  
 1-8-1 sandwich plates thermally loaded by the nonlinear temperature rise.

$T_t$	$p$	$\tilde{\omega}_1 (\Delta, \%)$	$\tilde{\omega}_2 = \tilde{\omega}_3 (\Delta, \%)$	$\tilde{\omega}_4 = \tilde{\omega}_5$	$\tilde{\omega}_6$	$\tilde{\omega}_7$	$\tilde{\omega}_8$	$\tilde{\omega}_9$	$\tilde{\omega}_{10}$
400 K	0.2	9.4089(4.33)	22.620(6.01)	33.590	34.859	42.580	42.583	47.489	53.578
		[39] 9.0180	21.3380						
	0.5	8.4056(4.31)	20.212(5.71)	29.665	31.142	38.039	38.046	41.958	47.854
		[39] 8.058	19.119						
	2	6.9779(3.28)	16.750(4.58)	23.767	25.750	31.415	31.423	33.636	39.449
[39] 6.756		16.016							
10	6.2364(2.66)	14.934(3.87)	20.588	22.967	27.910	27.916	29.127	34.984	
	[39] 6.075	14.378							
600 K	0.2	9.2157(5.82)	22.320(6.73)	33.278	34.447	42.118	42.142	47.105	53.018
		[39] 8.709	20.912						
	0.5	8.2261(5.65)	19.947(6.57)	29.723	30.783	37.646	37.668	41.671	47.377
		[39] 7.786	18.717						
	2	6.8079(4.34)	16.519(5.20)	23.589	25.447	31.099	31.121	33.484	39.065
[39] 6.525		15.700							
10	6.0752(3.74)	14.771(4.33)	20.394	22.608	27.592	27.609	28.924	34.593	
	[39] 5.856	14.101							
800 K	0.2	9.0275	22.035	33.030	34.058	41.687	41.727	46.761	52.496
	0.5	8.0516	19.690	29.188	30.439	37.275	37.312	41.412	46.923
	2	6.6437	16.292	23.381	25.140	30.785	30.818	33.336	38.672
	10	5.9216	14.479	20.111	22.275	27.244	27.255	28.691	34.134

**Table 8.** The first ten nondimensional frequencies of CCCC SUS304/Si<sub>3</sub>Ni<sub>4</sub> functionally graded square 1-8-1 sandwich plates thermally loaded by the nonlinear temperature rise.

$T_t$	$p$	$\tilde{\omega}_1 (\Delta, \%)$	$\tilde{\omega}_2 = \tilde{\omega}_3 (\Delta, \%)$	$\tilde{\omega}_4$	$\tilde{\omega}_5$	$\tilde{\omega}_6$	$\tilde{\omega}_7 = \tilde{\omega}_8$	$\tilde{\omega}_9 = \tilde{\omega}_{10}$
400 K	0.2	16.213(5.30)	31.190(7.63)	43.912	51.894	52.379	62.855	63.103
		[39] 15.397	28.977					
	0.5	14.460(5.20)	27.809(7.55)	39.144	46.248	46.683	55.893	56.110
		[39] 13.746	25.856					
600 K	0.2	11.929(3.99)	22.866(6.29)	32.118	37.881	38.248	45.286	45.880
		[39] 11.471	21.513					
	0.5	10.606(3.26)	20.265(5.59)	28.407	33.450	33.780	39.590	40.461
		[39] 10.271	19.192					
800 K	0.2	15.841(4.23)	30.664(7.22)	43.268	51.182	51.671	62.078	62.543
		[39] 15.199	28.598					
	0.5	14.102(3.73)	27.311(6.83)	38.541	45.586	46.025	55.278	55.719
		[39] 13.594	25.566					
10	0.2	11.566(1.62)	22.381(4.85)	31.545	37.258	37.631	44.221	45.195
		[39] 11.382	21.346					
	0.5	10.245(0.35)	19.783(3.63)	27.836	32.829	33.160	39.211	39.770
		[39] 10.210	19.09					

**Table 9.** The first nine nondimensional frequencies of two edges fully supported and two edges clamped (SCSC) SUS304/Si<sub>3</sub>Ni<sub>4</sub> functionally graded square 1-8-1 sandwich plates thermally loaded by the nonlinear temperature rise.

$T_t$	$p$	$\tilde{\omega}_1 (\Delta, \%)$	$\tilde{\omega}_2 (\Delta, \%)$	$\tilde{\omega}_3$	$\tilde{\omega}_4$	$\tilde{\omega}_5$	$\tilde{\omega}_6$	$\tilde{\omega}_7$	$\tilde{\omega}_8$	$\tilde{\omega}_9$
400 K	0.2	13.274(5.31)	24.512(6.55)	29.754	33.585	39.655	43.561	51.341	56.518	58.691
		[39] 12.605	23.014							
	0.5	11.846(5.25)	21.996(6.19)	26.537	29.655	35.380	38.897	45.768	50.435	51.944
		[39] 11.255	20.560							
600 K	0.2	9.7941(1.10)	18.105(5.34)	21.845	23.750	29.118	32.087	37.519	41.460	41.810
		[39] 9.402	17.187							
	0.5	8.7226(0.53)	16.116(4.65)	19.375	20.581	25.813	28.490	33.147	36.370	36.700
		[39] 8.425	15.400							
800 K	0.2	12.010(5.31)	24.201(7.36)	29.301	33.281	39.153	43.093	50.670	55.896	58.203
		[39] 12.354	22.542							
	0.5	11.597(4.99)	21.604(7.13)	26.118	29.388	34.922	38.481	45.185	49.877	51.524
		[39] 11.046	20.166							
10	0.2	9.5510(3.31)	17.840(5.62)	21.451	23.532	28.704	31.729	36.992	40.973	41.485
		[39] 9.245	16.89							
	0.5	8.4845(2.35)	15.855(4.68)	18.987	20.364	25.403	28.133	32.623	36.050	36.214
		[39] 8.290	15.146							

374 By inspecting Tables 7 to 9, one can observe that the first two frequencies obtained from the  
 375 present finite element model involving the 3D graded element are in a good agreement with the finite  
 376 element results reported in [39] for all the thermal and displacement boundary conditions considered  
 377 in the calculations. In addition, to show the effect of temperature on the natural frequencies of the SSSS  
 378 sandwich plates with different material gradients in SUS304/Si<sub>3</sub>Ni<sub>4</sub> cores, several nondimensional  
 379 frequencies from Table 7 are presented as a two-dimensional function of the temperature and the

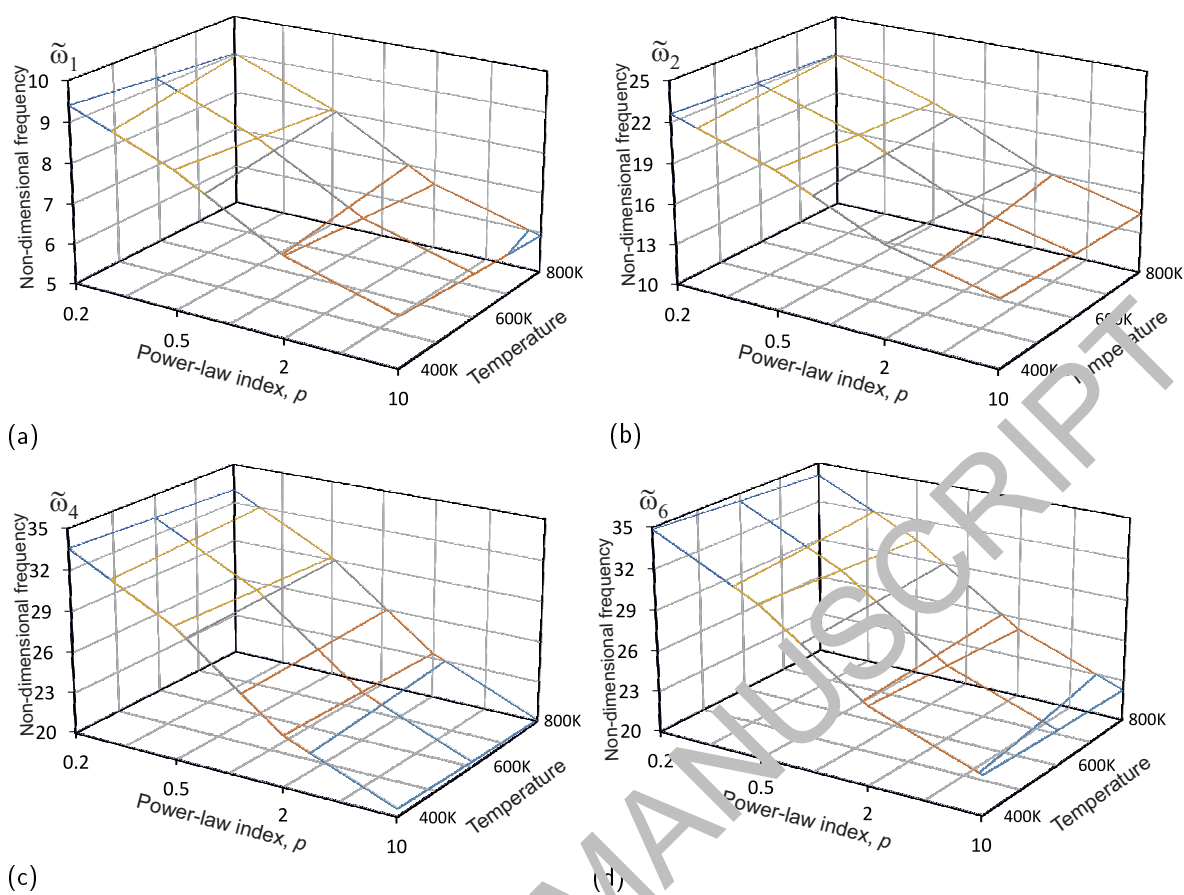


**Figure 7.** The effect of the temperature on natural frequencies of SSSS square 1-8-1 sandwich plates with different material gradients in  $\text{SiC}/\text{Si}_3\text{N}_4$  cores: **(a)** the first nondimensional frequency; **(b)** the second nondimensional frequency; **(c)** the fourth nondimensional frequency; and **(d)** the sixth nondimensional frequency.

power-law index in Figure 7. It is clearly seen from the plots that all the shown frequencies decrease with increasing temperature for each value of  $p$ , in other words, as expected, the FGM sandwich plates become more compliant because of the decrease in material stiffness at higher temperatures. Here, the variation of the volume fraction exponent affects the natural frequencies to a greater extent than the temperature in the considered range. It is also important to mention that the natural frequencies of the CCC and CSC sandwich plates exhibit similar responses with rising temperature, and by increasing the power-law index.

## 6. Conclusions

The free vibrations of FGM sandwich plates under temperature loading conditions are examined. The natural frequencies of thermally loaded FGM plates are computed using a model based on the 3D graded finite element developed within the ABAQUS code environment. The material gradient was assumed to vary in the thickness direction of the plates according to a power-law distribution of the volume fractions. The rule of mixture was used to evaluate the effective material properties of the FGM. The FGM was implemented into the conventional 3D elements of ABAQUS code via a combination of user-defined subroutines such as UMAT, UMATHT, and USDFLD (the codes can be downloaded from <http://polonez.pollub.pl/deliverables/>). In the simulations of FGM sandwich plates, the thermomechanical analysis, used to obtain a temperature profile and associated with temperature-induced displacement and stress fields, couples with a frequency analysis to calculate natural frequencies and mode shapes accounting for a temperature-defined base state. The latter

analysis adopted the average mass density instead of its spatial distribution adopted by the former one. The convergence analysis of the present FE model has been done to validate the accuracy of the numerical results by comparing them with the solutions previously reported in the literature and to estimate the model computational efficiency. The effects of different thermal loads, imposed at the external surfaces in steady-state conditions, and different displacement boundary conditions and material parameters, associated with a variety of volume fractions of the material constituents, on the frequencies of FGM sandwich plates are discussed in detail. The following conclusions can be drawn from the present study:

- The use of the graded finite elements for analyzing FGM sandwich plates provides a more efficient modeling approach than homogeneous elements to achieve high-fidelity results.
- The solutions of thermomechanical analysis reveal that a temperature profile calculated with the 3D model is important to predict correct thermal-induced displacement and stress distributions, which, in turn, affect the accuracy of calculated natural frequencies and mode shapes of thermally loaded FGM plates. The thermomechanical analysis also permits the mode shapes to be analyzed in terms of the temperature and stresses.
- It is observed from the simulations that the natural frequencies decrease as the volume fraction of ceramic decreases across the thickness of the FGM plates.
- The natural frequencies have a tendency to decrease with an increase of temperature for each of the functionally graded material profiles studied.
- This work forms a convenient tool for subsequent dynamic analyses of FGM sandwich plates under different temperature conditions with accurate finite element solutions provided by the ABAQUS commercial code.

The developed graded finite element can also be adopted to a 3D crack sensitivity analysis associated with nondestructive testing of FGM sandwich panels and welding-adhesive joints as proposed in [66,67]. This will be a subject of our future research.

**Author Contributions:** Conceptualization, V.N.B. and T.S.; methodology, V.N.B.; software, V.N.B. and S.D.; formal analysis, V.N.B. and S.D.; investigation, V.N.B.; validation, V.N.B. and S.D.; data curation, V.N.B.; writing—original draft preparation, V.N.B.; writing—review and editing, V.N.B., T.S., and S.D.; resources, T.S.; funding acquisition, V.N.B. and T.S.

**Funding:** This research was funded by the National Science Centre of Poland at the Lublin University of Technology within POLONEZ 2 program grant number UMO-2016/21/P/ST8/00790 supported by the European Union's Horizon 2020 research and innovation program under the Marie Skłodowska-Curie grant agreement number 665778.

**Conflicts of Interest:** The authors declare no conflict of interest.

## References

1. Anraei, M.; Shahravi, M.; Noori, Z.; Lenjani, A. Application of aluminium honeycomb sandwich panel as an energy absorber of high-speed train nose. *J. Compos. Mater.* **2014**, *48*, 1027–1037. <https://doi.org/10.1177/0021998313482019>
2. Manalo, A.; Aravinthan, T.; Fam, A.Z.; Benmokrane B. State-of-the-art review on FRP sandwich systems for lightweight civil infrastructure. *J. Compos. Construct.* **2017**, *21*, 16 pages. [https://doi.org/10.1061/\(ASCE\)CC.1943-5614.0000729](https://doi.org/10.1061/(ASCE)CC.1943-5614.0000729)
3. Han, B.; Zhang, Z. J.; Zhang, Q. C.; Zhang, Q.; Lu, T. J.; Lu, B.H. Recent advances in hybrid lattice-cored sandwiches for enhanced multifunctional performance. *Mater. Design* **2017**, *10*, 58–69. <https://doi.org/10.1016/j.eml.2016.11.009>
4. Altenbach, H.; Altenbach, J.; Kissing, W. *Mechanics of Composite Structural Elements*; 2nd edn.; Springer Nature: Singapore, Malaysia, 2018, pp. 470.
5. Lu, C.; Zhao, M.; Jie, L.; Wang, J.; Gao, Y.; Cui, X.; Chen, P. Stress distribution on composite honeycomb sandwich structure suffered from bending load. *Procedia Eng.* **2015**, *99*, 405–412. <https://doi.org/10.1016/j.proeng.2014.12.554>

- 448 6. Szekrényes, A. Analytical solution of some delamination scenarios in thick structural sandwich plates. *J.*  
 449 *Sandw. Struct. Mater.* **2019**, *21*(4), 1271–1315. <https://doi.org/10.1177/1099636217714182>
- 450 7. Burlayenko, V.N.; Sadowski, T.; Pietras, D. A numerical analysis of near tip fields in a bending  
 451 moment-loaded double cantilever sandwich beam fracture specimen. *Bull. NTU "KhPI". Ser. Math.*  
 452 *Model. Eng. Technol.* **2018**, *3*, 9–14. [http://nbuv.gov.ua/UJRN/vcpimm\\_2018\\_3\\_4](http://nbuv.gov.ua/UJRN/vcpimm_2018_3_4)
- 453 8. Shi, S.-S.; Sun, Z.; Hu, X.-Z.; Chen, H.-R. Carbon-fiber and aluminum-honeycomb sandwich composites  
 454 with and without Kevlar-fiber interfacial toughening. *Compos. Part A - Appl. Sci. Manuf.* **2017**, *67*, 102–110.  
 455 <https://doi.org/10.1016/j.compositesa.2014.08.017>
- 456 9. Burlayenko, V.N.; Pietras, D.; Sadowski, T. Influence of geometry, elasticity properties and boundary  
 457 conditions on the Mode I purity in sandwich composites. *Compos. Struct.* **2019**, *203*. (in press, <https://doi.org/10.1016/j.compstruct.2019.110942>
- 458 <https://doi.org/10.1016/j.compstruct.2019.110942>
- 459 10. Magnucki, K.; Jasion, P.; Szyk, W.; Smyczynski, M.J. Strength and buckling of a sandwich beam with  
 460 thin binding layers between faces and a metal foam core. *Steel Compos. Struct.* **2014**, *16*, 325–337. <https://doi.org/10.12989/scs.2014.16.3.325>
- 461 <https://doi.org/10.12989/scs.2014.16.3.325>
- 462 11. Juhász, Z.; Szekrényes, A. The effect of delamination on the critical buckling force of composite plates:  
 463 Experiment and simulation. *Compos. Struct.* **2017**, *168*, 456–464. [https://doi.org/10.1016/j.compstruct.2017.](https://doi.org/10.1016/j.compstruct.2017.02.052)  
 464 [02.052](https://doi.org/10.1016/j.compstruct.2017.02.052)
- 465 12. Burlayenko V.N.; Sadowski, T. Numerical modeling of sandwich plates with partially debonded skin-to-core  
 466 interface for damage detection. In Proceedings of the 8th International Conference on Structural Dynamics  
 467 (EURODYN 2011), Leuven, Belgium, 4-10 July, 2011; De Roeck, G., Degrande, G., Lombaert, G., Muller, G.  
 468 Eds.; pp. 2242–2249, 116680.
- 469 13. Burlayenko, V.N.; Sadowski, T. Dynamic analysis of debonded sandwich plates with flexible core – Numerical  
 470 aspects and simulation. In *Shell-like Structures*; Altenbach, H., Eremeyev, V.A., Eds.; *Adv. Struct. Mater.*, *15*;  
 471 Springer: Heidelberg, Germany, 2011; pp. 415–440. [https://doi.org/10.1007/978-3-642-21855-2\\_27](https://doi.org/10.1007/978-3-642-21855-2_27)
- 472 14. Jayatilake, I. N.; Karunasena, W.; Lokuge, W. Finite element based dynamic analysis of multilayer fibre  
 473 composite sandwich plates with interlayer delaminations. *Adv. Aircr. Spacecr. Sci., Int. J.* **2016**, *3*, 15–28.  
 474 <http://dx.doi.org/10.12989/aas.2016.3.1.015>
- 475 15. Savin-Barcan, M.; Beznea, E.-F.; Chiriac, T. Influence of fabrication imperfections on dynamic response of  
 476 a sandwich composite panel of a ship deck structure. *IOP Conf. Ser. Mater. Sci. Eng.* **2018**, *400*, 032008.  
 477 <https://doi.org/10.1088/1757-899X/400/3/032008>
- 478 16. Burlayenko, V.N.; Sadowski, T. Transient dynamic response of debonded sandwich plates predicted with  
 479 finite element analysis. *Mechanica* **2014**, *49*, 2617–2633. <https://doi.org/10.1007/s11012-014-9924-y>
- 480 17. Qu, Y.; Meng, G. Nonlinear vibro-acoustic analysis of composite sandwich plates with skin-core debondings.  
 481 *AIAA J.* **2017**, *55*, 1723–1733. <https://doi.org/10.2514/1.J055489>
- 482 18. Idriss, M.; El Mahi, A. Effects of debonding length on the fatigue and vibration behaviour of sandwich  
 483 composite. *J. Compos. Mater.* **2017**, *51*, 1839–1847. <https://doi.org/10.1177/0021998316663292>
- 484 19. Burlayenko, V.N.; Sadowski, T. Linear and nonlinear dynamic analyses of sandwich panels with face  
 485 sheet-to-core debonding. *Shock Vib.* **2018**, *2018*, Article ID 5715863, 26 pages. [https://doi.org/doi:10.1155/](https://doi.org/doi:10.1155/2018/5715863)  
 486 [2018/5715863](https://doi.org/doi:10.1155/2018/5715863)
- 487 20. Burlayenko, V.N.; Sadowski, T. Simulations of post-impact skin/core debond growth in sandwich plates  
 488 under impulsive loading. *J. Appl. Nonlin. Dyn.* **2014**, *3*(4), 369–379. [10.5890/JAND.2014.12.008](https://doi.org/10.5890/JAND.2014.12.008)
- 489 21. Lunari, M.F.; Greco, F.; Lonetti, P. Sandwich panels under interfacial debonding mechanisms. *Compos. Struct.*  
 490 **2018**, *203*, 310–320. <https://doi.org/10.1016/j.compstruct.2018.06.113>
- 491 22. Burlayenko, V.N.; Altenbach, H.; Sadowski, T. Dynamic fracture analysis of sandwich composites with  
 492 face sheet/core debond by the finite element method. In *Dynamical Processes in Generalized Continua and*  
 493 *Structures* Altenbach, H., Belyaev, A., Eremeyev, V.A., Krivtsov, A., Porubov, A.V., Eds.; *Adv. Struct. Mater.*,  
 494 *103*; Springer Nature: Cham, Switzerland, 2019; pp. 163–194. [https://doi.org/10.1007/978-3-030-11665-1\\_9](https://doi.org/10.1007/978-3-030-11665-1_9)
- 495 23. Zenkour, A.M. A comprehensive analysis of functionally graded sandwich plates: part 1-Deflection and  
 496 stresses. *Int. J. Solids Struct.* **2005**, *42*, 5224–5242. <https://doi.org/10.1016/j.ijsolstr.2005.02.015>
- 497 24. Kanu, N.J.; Vates, U.K.; Singh, G.K.; Chavan, S. Fracture problems, vibration, buckling, and bending analyses  
 498 of functionally graded materials: A state-of-the-art review including smart FGMS. *Particul. Sci. Technol.* **2019**,  
 499 *37*(5), 579–604. <https://doi.org/10.1080/02726351.2017.1410265>

- 500 25. Ghazaryan, D.; Burlayenko, V.N.; Avetisyan, A.; Bhaskar A. Free vibration analysis of functionally graded  
501 beams with non-uniform cross-section using the differential transform method. *J. Eng. Math.* **2018**, *110*,  
502 97–121. <https://doi.org/10.1007/s10665-017-9937-3>
- 503 26. Li, C.; Shen, H.-S.; Wang, H. Nonlinear dynamic response of sandwich beams with functionally graded  
504 negative Poisson's ratio honeycomb core. *Eur. Phys. J. Plus* **2019** *134*, 15 pages. <https://doi.org/10.1140/epjp/i2019-12572-7>
- 505 27. Vakili-TAHAMI, F.; Mahkam, N.; Fard, A.M.A. Optimum design of functionally graded plates under thermal  
506 shock. *UPB Sci. Bull. Ser. D: Mechan. Eng.* **2017**, *79*(3), 69–88.
- 507 28. Do, T.V.; Bui, T.Q.; Yu, T.T.; Pham, D.T.; Nguyen, C.T. Role of material combination and new results of  
508 mechanical behavior for FG sandwich plates in thermal environment. *J. Comput. Sci.* **2017**, *21*, 164–181.  
509 <http://dx.doi.org/10.1016/j.jocs.2017.06.015>
- 510 29. Petrova, V.; Schmauder, S. Modeling of thermo-mechanical fracture of FGMs with respect to multiple cracks  
511 interaction. *Phys. Mesomech.* **2017**, *20*, 241–249. <https://doi.org/10.1134/S1029959917030008>
- 512 30. Burlayenko, V.N. Modelling thermal shock in functionally graded plates with finite element method. *Adv.*  
513 *Mater. Sci. Eng.* **2016**, *2016*, Article ID 7514638, 12 pages. <http://dx.doi.org/10.1155/2016/7514638>
- 514 31. Pathak, H. Three-dimensional quasi-static fatigue crack growth analysis in functionally graded materials  
515 (FGMs) using coupled FE-XEFG approach. *Theor. Appl. Fract. Mec.* **2017**, *92*, 59–75. <https://doi.org/10.1016/j.tafmec.2017.05.010>
- 516 32. Ivanov, I.; Velchev, D.; Penkova, N.; Krumov, K.; Iliev, V. Stress analysis of insulating glass units under  
517 transient thermal loadings. *J. Chem. Technol. Metall.* **2018**, *53*(6), 1095–1102.
- 518 33. Zhang, H.H.; Han, S.Y.; Fan, L.F.; Huang, D. The numerical manifold method for 2D transient heat conduction  
519 problems in functionally graded materials. *Eng. Anal. Bound. Elem.* **2018**, *88*, 145–155. <https://doi.org/10.1016/j.enganabound.2018.01.003>
- 520 34. Swaminathan, K.; Sangeetha, D.M. Thermal analysis of FGM plates – A critical review of various modeling  
521 techniques and solution methods. *Compos. Struct.* **2017**, *160*, 43–70. <https://doi.org/10.1016/j.compstruct.2016.10.047>
- 522 35. Reddy, J. N. Analysis of functionally graded plates. *Int. J. Numer. Meth. Eng.* **2000**, *47*, 663–384.
- 523 36. Matsunaga, H. Free vibration and stability of angle-ply laminated composite and sandwich plates under  
524 thermal loading. *Compos. Struct.* **2005**, *77*, 249–262. <https://doi.org/10.1016/j.compstruct.2005.07.002>
- 525 37. Zenkour, A.M. The effect of transverse shear and normal deformations on the thermomechanical bending  
526 of functionally graded sandwich plates. *Int. J. Appl. Mech.* **2009**, *1*(4), 667–707. <https://doi.org/10.1142/S1758825109000368>
- 527 38. Fazzolari, F.A. Natural frequencies and critical temperatures of functionally graded sandwich plates subjected  
528 to uniform and non-uniform temperature distributions. *Compos. Struct.* **2015**, *121*, 197–210. <https://doi.org/10.1016/j.compstruct.2014.10.039>
- 529 39. Pandey S.; Pradyumna S. Free vibration of functionally graded sandwich plates in thermal environment using  
530 a layerwise theory. *Eur. J. Mech. A-Solid* **2015**, *51*, 55–66. <https://doi.org/10.1016/j.euromechsol.2014.12.001>
- 531 40. Mantar, J. L.; Cranados, E. V. Thermoelastic behavior of advanced composite sandwich plates by using a  
532 new boundary in quasi-3D hybrid type HSDT. *Compos. Struct.* **2015**, *126*, 132–144. <https://doi.org/10.1016/j.compstruct.2015.01.055>
- 533 41. Do, T.N.V.; Lee, C.-H. Quasi-3D higher-order shear deformation theory for thermal buckling analysis of  
534 FGM plates based on a meshless method. *Aerosp. Sci. Technol.* **2018**, *82–83*, 450–465. <https://doi.org/10.1016/j.ast.2018.09.017>
- 535 42. Han, B.; Hui, W.-W.; Zhang, Q.-C.; Zhao, Z.-Y.; Jin, F.; Zhang, Q.; Lu, T.J.; Lu, B.-H. A refined quasi-3D  
536 zigzag beam theory for free vibration and stability analysis of multilayered composite beams subjected to  
537 thermomechanical loading. *Compos. Struct.* **2018**, *204*, 620–633. <https://doi.org/10.1016/j.compstruct.2018.08.005>
- 538 43. Reddy, J.N.; Cheng, Z.-Q. Frequency of functionally graded plates with three-dimensional asymptotic  
539 approach. *J. Eng. Mech.* **2003**, *129*(8), 896–900. [https://doi.org/10.1061/\(ASCE\)0733-9399\(2003\)129:8\(896\)](https://doi.org/10.1061/(ASCE)0733-9399(2003)129:8(896))
- 540 44. Reddy, J.N.; Chen, Z.-Q. Three-dimensional thermomechanical deformations of functionally graded  
541 rectangular plates. *Eur. J. Mech. A-Solids* **2001**, *20*, 841–855. [https://doi.org/10.1016/S0997-7538\(01\)01174-3](https://doi.org/10.1016/S0997-7538(01)01174-3)
- 542 45. Vel, S.S.; Batra, R.C. Three-dimensional analysis of transient thermal stresses in functionally graded plates.  
543 *Int. J. Solids Struct.* **2003**, *40*, 7181–7196. [https://doi.org/10.1016/S0020-7683\(03\)00361-5](https://doi.org/10.1016/S0020-7683(03)00361-5)

- 553 46. Li, Q.; Iu, V.P.; Kou, K.P. Three-dimensional vibration analysis of functionally graded material plates in  
554 thermal environment. *J. Sound Vibr.* **2009**, *324*, 733–750. <https://doi.org/10.1016/j.jsv.2009.02.036>
- 555 47. Alibeigloo, A. Exact solution for thermo-elastic response of functionally graded rectangular plates. *Compos.*  
556 *Struct.* **2010**, *92*, 113–121. <https://doi.org/10.1016/j.compstruct.2009.07.003>
- 557 48. Brischetto, S.; Torre, R. 3D shell model for the thermo-mechanical analysis of FGM structures via imposed  
558 and calculated temperature profiles. *Aerosp. Sci. Technol.* **2019**, *85*, 125–149. <https://doi.org/10.1016/j.ast.2018.12.011>
- 559  
560 49. Zhang, Z.(Jenny); Paulino, G.H. Wave propagation and dynamic analysis of smoothly graded heterogeneous  
561 continua using graded finite elements. *Int. J. Solids Struct.* **2007**, *44*(11–12), 3601–3626. <https://doi.org/10.1016/j.ijsolstr.2005.05.061>
- 562  
563 50. Asemi, K.; Salehi, M.; Akhlaghi, M. Three dimensional graded finite element elasticity shear buckling analysis  
564 of FGM annular sector plates. *Aerosp. Sci. Technol.* **2015**, *43*, 1–13. <https://doi.org/10.1016/j.ast.2015.02.009>
- 565 51. Santare, M.H.; Thamburaj, P.; Gazonas, G.A. The use of graded finite elements in the study of elastic wave  
566 propagation in continuously nonhomogeneous materials. *Int. J. Solids Struct.* **2003**, *40*(21), 5621–5634.  
567 [https://doi.org/10.1016/S0020-7683\(03\)00315-9](https://doi.org/10.1016/S0020-7683(03)00315-9)
- 568 52. Brischetto, S.; Carrera, E. Coupled thermo-mechanical analysis of one-layered and multilayered plates.  
569 *Compos. Struct.* **2010**, *92*, 1793–1812. <https://doi.org/10.1016/j.compstruct.2010.01.020>
- 570 53. Bui, T.Q.; Do, T.V.; Ton, L.H.T.; Doan, D.H.; Tanaka, S.; Pham, D.T.; Nguyen-van, T.-A.; Yu, T.; Hirose,  
571 S. On the high temperature mechanical behaviors analysis of heated functionally graded plates using  
572 FEM and a new third-order shear deformation plate theory. *Compos. Part B-Eng.* **2016**, *92*(1), 218–241.  
573 <http://dx.doi.org/10.1016/j.compositesb.2016.02.048>
- 574 54. Pandey, S.; Pradyumna, S. Transient stress analysis of sandwich plate and shell panels with functionally  
575 graded material core under thermal shock. *J. Therm. Stresses* **2018**, *41*(5), 543–567. <https://doi.org/10.1080/01495739.2017.1422999>
- 576  
577 55. Moleiro, F.; Franco Correia, V.M.; Ferreira, A.J.M.; Pedry, J.N. Fully coupled thermo-mechanical analysis  
578 of multilayered plates with embedded FGM skins or core layers using a layerwise mixed model. *Compos.*  
579 *Struct.* **2019**, *210*, 971–996. <https://doi.org/10.1016/j.compstruct.2018.11.073>
- 580 56. *ABAQUS User's manual ver. 2016*. Dassault Systèmes Simulia Corp., Providence, RI, USA, 2016.
- 581 57. Reinoso, J.; Blázquez, A. Geometrically non-linear analysis of functionally graded power-based and carbon  
582 nanotubes reinforced composites using a fully integrated solid shell element. *Compos. Struct.* **2016**, *152*,  
583 277–294. <https://doi.org/10.1016/j.compstruct.2016.05.036>
- 584 58. Buttlar, W.G.; Paulino, G.H.; Song, S.M. Application of graded finite elements for asphalt pavements. *J. Eng.*  
585 *Mech.* **2006**, *132*(3), 240–248. [https://doi.org/10.1061/\(ASCE\)0733-9399\(2006\)132:3\(240\)](https://doi.org/10.1061/(ASCE)0733-9399(2006)132:3(240))
- 586 59. Burlayenko, V.N.; Altenbach, H.; Sadowski, T.; Dimitrova, S.D.; Bhaskar, A. Modelling functionally graded  
587 materials in heat transfer and thermal stress analysis by means of graded finite elements. *Appl. Math. Model.*  
588 **2017**, *45*, 422–438. <https://doi.org/10.1016/j.apm.2017.01.005>
- 589 60. Mars, J.; Kouba, S.; Wali, M.; Dammak, F. Numerical analysis of geometrically non-linear behavior of  
590 functionally graded shells. *Lat. Am. J. Solids Struct.* **2017**, *14*(11), 1952–1978. <http://dx.doi.org/10.1590/1679-7825.2017.14.1952>
- 591  
592 61. Saiyekar, S.M.; Lavate, P. Flexure of power law governed functionally graded plates using ABAQUS UMAT.  
593 *Aerosp. Sci. Technol.* **2015**, *46*, 51–59. <https://doi.org/10.1016/j.ast.2015.06.021>
- 594 62. Burlayenko, V.N.; Sadowski, T. Free vibrations and static analysis of functionally graded sandwich plates with  
595 three-dimensional finite elements. *Meccanica* **2019**. (in press) <https://doi.org/10.1007/s11012-019-01001-7>
- 596 63. Burlayenko, V.N.; Altenbach, H.; Sadowski, T.; Dimitrova, S.D. Three-dimensional finite element modelling  
597 of free vibrations of functionally graded sandwich panels. In *Recent Developments in the Theory of Shells*  
598 Altenbach, H., Chróścielewski, J., Eremeyev, V.A., Wiśniewski, K., Eds.; *Adv. Struct. Mater.*, 110; Springer  
599 Nature: Cham, Switzerland, 2019. (in press) [https://doi.org/10.1007/978-3-030-17747-8\\_10](https://doi.org/10.1007/978-3-030-17747-8_10)
- 600 64. Hetnarski, R.B.; Eslami, M.R. *Thermal Stresses - Advanced Theory and Applications*. Springer, Science+Business  
601 Media, B.V., 2009.
- 602 65. Sutradhar, A.; Paulino, G.H. The simple boundary element method for transient heat conduction in  
603 functionally graded materials. *Comput. Methods Appl. Mech. Eng.* **2004**, *193*, 4511–4539. <https://doi.org/10.1016/j.cma.2004.02.018>
- 604

- 605 66. Gajewski, J.; Sadowski T. Sensitivity analysis of crack propagation in pavement bituminous layered structures  
606 using a hybrid system integrating Artificial Neural Networks and Finite Element Method. *Comp. Mater. Sci.*  
607 **2014**, *82*, 114–117. <https://doi.org/10.1016/j.commatsci.2013.09.025>
- 608 67. Sadowski, T.; Kneć, M.; Golewski, P. Experimental investigation and numerical modelling of spot  
609 welding-adhesive joints response. *Compos. Struct.* **2014**, *112*, 66–77. [https://doi.org/10.1016/j.compstruct.](https://doi.org/10.1016/j.compstruct.2014.01.008)  
610 [2014.01.008](https://doi.org/10.1016/j.compstruct.2014.01.008)

ACCEPTED MANUSCRIPT